ACS OMEGA

Open Access

http://pubs.acs.org/journal/acsodf

Article

On-Chip Polarization Rotators Using Metasurface

Dura Shahwar,* Markku Kapulainen, Tomi Haatainen, Mikko Harjanne, Matteo Cherchi, Zhipei Sun, Timo Aalto, and Kirsi Tappura*

Cite This: *ACS Omega* 2024, 9, 33055−33063

Read Online

ACCESS | Metrics & More | Article Recommendations

ABSTRACT: Metasurfaces, with their ability to finely manipulate light properties (e.g., polarization), represent a frontier in optical technology. Here, we report innovative gold-based metasurfaces that are adept at changing the light polarization across a broad range of incident angles. Their expansive acceptance angle facilitates seamless integration with silicon waveguides, culminating in the realization of a novel, compact, broadband, and low-loss on-chip polarization rotator. The demonstrated metasurface devices show polarization conversion efficiencies as high as 98.5% at 1550 nm in the free space measurements. Unlike conventional plasmonic metasurfaces, which lack broadband capabilities, our metasurface-based waveplates show extinction ratios of >15 dB for a 120 nm bandwidth. These metasurfaces are positioned on top of up-reflecting mirrors fabricated in a micrometer-scale silicon-on-insulator platform to demonstrate on-chip polarization rotation. The demonstrated polarization rotator shows an extinction ratio of more than 10 dB for a 100 nm bandwidth. This study marks the first successful demonstration of on-chip polarization manipulation utilizing metasurface integration, heralding significant potential impacts for enhancing the functionality and miniaturization of photonic integrated circuits.

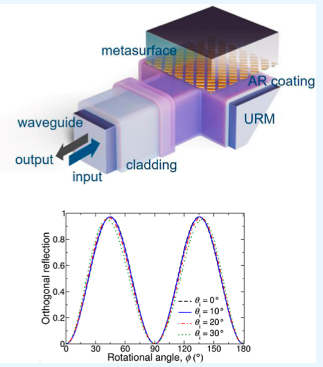

1. INTRODUCTION

Metasurfaces, two-dimensional analogues of metamaterials, have emerged as an attractive alternative to bulk metamaterials due to their lower losses and reduced fabrication challenges. They have exhibited remarkable capabilities of manipulating light, typically its phase and polarization properties,[1−4] with surface-confined structures and subwavelength spatial resolutions. These unique properties of metasurfaces have been used to demonstrate a variety of devices and novel physical phenomena, such as meta-lenses,[5,6] holography,[7] invisible cloaks,[8] optical spin hall effect,[9] polarization converters, polarizers, and polarization-manipulating waveplates,[10−16] Among the polarization control applications related to plasmonic metasurfaces, there has been a rapid rise in the designs of broadband reflective waveplates with high polarization conversion ratios and a wide field of view compared to conventional birefringent materials.[13] These high polarization conversion efficiencies (PCEs) can support the development of polarization management building blocks such as polarization rotators (PR) and splitters.

Polarization management devices play a key role in photonic integrated circuits (PICs).[17] Among PICs, silicon photonics is one of the most promising integration approaches for optics: it is versatile and widely used with multiple flavors. Silicon photonics platforms can be based on so-called thick or thin silicon-on-insulator (SOI) waveguides or even silicon nitride waveguides.[18] While thin-SOI waveguides typically have a 200−300 nm thick Si core, the thick-SOI waveguide platform used in this work has a 3 μm thick Si core. Thick SOI is well-known for its low optical losses (a few dB per meter or even less), suitability for ultradense integration (low loss), and small polarization dependence. Most of the building blocks of the thick-SOI platform support both polarizations, i.e., TE and TM polarized modes, but there is a challenge when the two polarizations need to be treated independently, for example, in telecom and sensing applications.[19]

Most of the conventional approaches for on-chip polarization management are developed for thin waveguides made on submicrometer thick layers of silicon (Si), silicon nitride (Si_3N_4), or compound semiconductor materials. In particular, conventional methods to generate reciprocal polarization rotations in SOI platforms are based on mode conversion[20,21] and mode evolution.[22] A simple mode-evolution-based polarization rotator utilizes adiabatic structures to change the mode in the waveguide, which usually leads to a long device. In contrast, mode interference or mode coupling uses the beating between two modes of hybrid polarization to minimize the device length. PR developed for thin-SOI platforms have been reported to exhibit insertion losses of about 1 dB.[23] However, designing these building blocks requires careful consideration,

Received: April 30, 2024
Revised: June 15, 2024
Accepted: July 9, 2024
Published: July 20, 2024

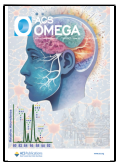

and the most commonly used approaches are not well-suited to 3 μm thick SOI waveguides.

The efforts for developing polarization management components for thick-SOI platforms have been limited, because it is hard to achieve the required phase shifts between the two orthogonal modes. However, for a micron-scale InP platform, a polarization splitter−rotator was reported with an extinction ratio of more than 14 dB for a 1550 ± 10 nm wavelength.[24] For a micron-scale silicon photonics platform, so far, we have only demonstrated on-chip polarization splitters.[25] Further, a new design concept has recently been proposed for polarization splitters and rotators based on an elegant approach using a v-groove-assisted design for micron-scale silicon photonics, but still to be experimentally demonstrated.[26] Even though typical solutions operate in the transmission mode, a recent study proposes a corrugated waveguide design for a reflective polarization rotator in thin SOI with a PCE of 93.1% for a 9.21 μm long device.[27] There is also a report on a thin-SOI integrated plasmonic waveplate based on an asymmetric hybrid plasmonic waveguide with a demonstrated PCE of 91.5% for a bandwidth of 60 nm.[28] Another elegant approach to achieve polarization rotation using twisted waveguide approach has been demonstrated with 90% PCE at 1550 nm.[29]

While meta-waveguides have been developed for polarization manipulation applications using metamaterials[30,31] to date, polarization manipulating metasurfaces have been demonstrated to work for free-space applications only. The combinations of metasurfaces and PICs have been studied, but present demonstrations focus on light-out coupled off-chip applications,[32] such as optical sensing and communication, including even switchable wavefront shaping.[33] A recent study shows how metasurface-integrated on-chip can accurately change the phase and amplitude of free-space emissions for structured beams and holography applications.[34] The emergence of metasurfaces has addressed key challenges that are difficult to solve with traditional optical devices. However, integration of metasurfaces on-chip is limiting its realization for high-volume, low-cost devices due to the requirement of nanolithography and transferring fragile films.[35] On-chip metasurfaces may also suffer from coupling efficiencies which is crucial for PR and waveguide devices.[36]

To the best of our knowledge, there are no demonstrations of a waveguide-integrated metasurface applied to on-chip polarization manipulation. Here, we show that the unique features of metasurfaces can be tailored for waveguide applications, specifically for polarization management in silicon photonics. We propose and demonstrate a novel approach that integrates a metasurface-based reflective plasmonic waveplate on top of an upreflective mirror (URM) to realize compact and broadband polarization rotating devices on the 3 μm SOI platform. The nanostructured plasmonic metasurfaces are based on gold (Au) nanorods, and they rotate the polarization of reflected light by the amount defined by the rotational orientation of the metasurface with respect to the incoming light. When placed on top of a URM, the metasurface acts as a reflective waveplate. The URMs are based on total internal reflection, and they are used for coupling light in and out of the chip or wafer on the 3 μm SOI platform with ∼1 dB coupling losses.[37]

The use of a conventional waveplate on top of a URM is limited by the divergence of light within the waveplate. To achieve efficient coupling from a reflective waveplate back to the URM without any focusing optics, the total thickness of the waveplate should be less than the mode-field diameter to limit diffraction losses. Conventional waveplates are much thicker than this because of the limited birefringence achievable in ordinary crystalline materials. Such limitations can be overcome by designing a suitable metasurface. The fabricated Au metasurfaces, i.e., metasurface-based waveplates, show PCE of 98.5% at 1550 nm and more than 91% for the wide wavelength range under study (1480−1630 nm). When integrated with silicon waveguides via URMs, the resulting PR show polarization extinction ratios (PER) of about 10 dB for a bandwidth of 120 nm, verifying the first-of-its-kind on-chip polarization rotator using metasurfaces integrated with SOI waveguides.

2. OUR CONCEPT OF METASURFACE-BASED ON-CHIP POLARIZATION MANAGEMENT

Figure 1 shows a schematic presentation of the proposed metasurface-based waveplate device for 90° polarization rotation on top of a URM. The structure consists of a top anisotropic metasurface (Au nanorods), an intermediate silicon dioxide (SiO_2) layer, and an Au layer serving as a back reflector. The intermediate silicon dioxide layer and bottom gold layer provide additional degrees of freedom for adjusting the phase and amplitude of the reflected waves, which in turn enables enhancing the bandwidth performance of the proposed metasurface device.

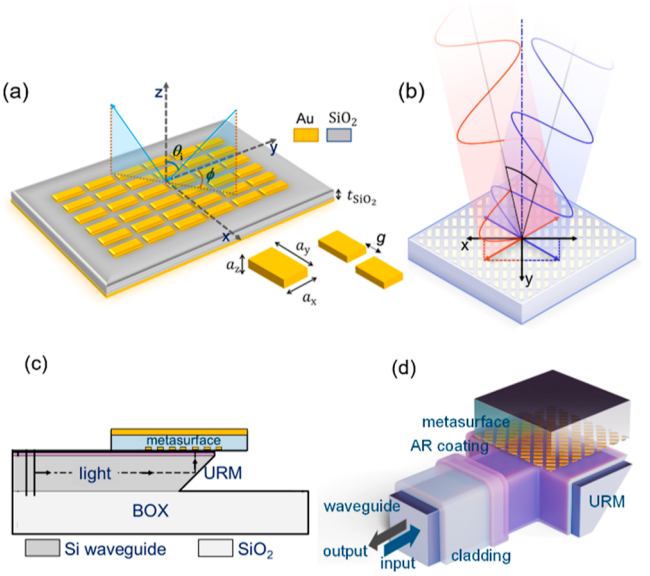

Figure 1. Our concept of metasurface-based on-chip polarization management. (a) Schematic presentation of the proposed Au-based metasurface for a 90° polarization rotation. (b) Illustration showing an incoming wave (red) and the reflected one (blue) with its polarization mirrored with respect to the main (y) axis of the metasurface. (c) Cross-sectional and (d) 3D schematic of our proposed metasurface-based on-chip polarization management device. A 45° URM in the Si waveguide is used to integrate with a metasurface on top. AR indicates antireflection.

In our metasurface design concept, an s-polarized (p-polarized) plane wave is incident on the metasurface at an angle marked with θ_i and the goal is to have only a p-polarized (s-polarized) plane wave reflected back from the metasurface. When the incident light interacts with the metasurface, light

https://doi.org/10.1021/acsomega.4c04158
ACS Omega 2024, 9, 33055−33063

undergoes multiple reflections between the metasurface and the bottom Au reflector. After interference, the final reflected wave is formed. The anisotropic scattering by the nanorods creates a large phase difference between the two orthogonally polarized modes over a broad wavelength range. This introduces the phase shift required for the waveplate operation, similar to that reported previously for a metasurface designed for smaller wavelengths (640−1290 nm).[13]

Figure 1a shows the basic structure and relevant dimensions of the metasurface device: a_x is the width, a_y is the length and a_z is the height of the single nanorod, whereas g is the interelement gap between the nanorods in the y direction and t_{SiO2} is the thickness of the dielectric layer between the nanorods and the planar gold reflector. The operational principle as a waveplate is sketched in Figure 1b, showing how the polarization is reflected with respect to the eigenaxis of the metasurface. To achieve 90° polarization rotation, the input polarization is set at a 45° angle (ϕ = 45°) with respect to the eigenaxis of the metasurface (i.e., the longer axis of the nanorods or the y-axis in Figure 1a). As a result, both eigenmodes are excited equally, and in the ideal case, the metasurface induces a 180° phase shift between them, similar to the operation of a conventional waveplate. Finally, Figure 1c,d illustrate the integration of the metasurface to a silicon photonics waveguide mirror for implementing the proposed integrated metasurface-based PR. The waveguide test structure consists of a rib waveguide at the input followed by a rib-to-strip converter, Euler bend and URM. The Euler bend ensures single-mode operation even if it is realized in a multimode strip waveguide, which is adiabatically coupled to a single-mode rib waveguide using a rib-strip converter. The rib waveguide is single mode over an ultrawide wavelength range (1.2−4 μm).[37]

As will be shown later in this paper, the designed metasurface works with high efficiency over a broad range of angles of incidence (θ_i), i.e., with a field of view ($2\theta_i$) of more than 65°. This allows one to cope with the finite divergence of light when it propagates twice through the URM, the gap between the URM and the metasurface, and the metasurface itself. In fact, the far-field half angle of the light emitted from the URM is 15 ± 1°, and by using the ultrathin metasurface as a waveplate, the real divergence angle can be kept much smaller than this.

3. RESULTS AND DISCUSSION

3.1. Concept Designs. To demonstrate the performance of our on-chip polarization rotator, we first designed Au-nanorod-based metasurfaces for a 1550 nm wavelength. a_x, a_y, a_z, g, p_x, and t_{SiO2} are the design parameters defining the metasurface operation. The values for the parameters are selected, based on three-dimensional (3D) full-wave electromagnetic simulations, to achieve a 90° polarization rotation with minimal absorption in the nanorods. A close-to-optimal performance was obtained for the following parameter set: t_{SiO2} = 160 nm, g = 16−25 nm, p_x = 252 nm, a_x = 90 nm, a_y = 262 nm − g, and a_z = 50 nm. Figure 2a shows the simulated power relative to the incident power, reflected from a metasurface waveplate to the polarization orthogonal to that of the incident wave as a function of the rotational angle (ϕ) of the metasurface. An efficient 90° rotation of the polarization is seen at angles of ϕ = 45° and ϕ = 135°. Absorption losses in the nanorods (in Au and the Ti adhesion layer underneath Au) are small but non-negligible, i.e., less than 5.5% at the maximum (at ϕ = 0° and ϕ = 180°) and near 3.5% at ϕ = 45°

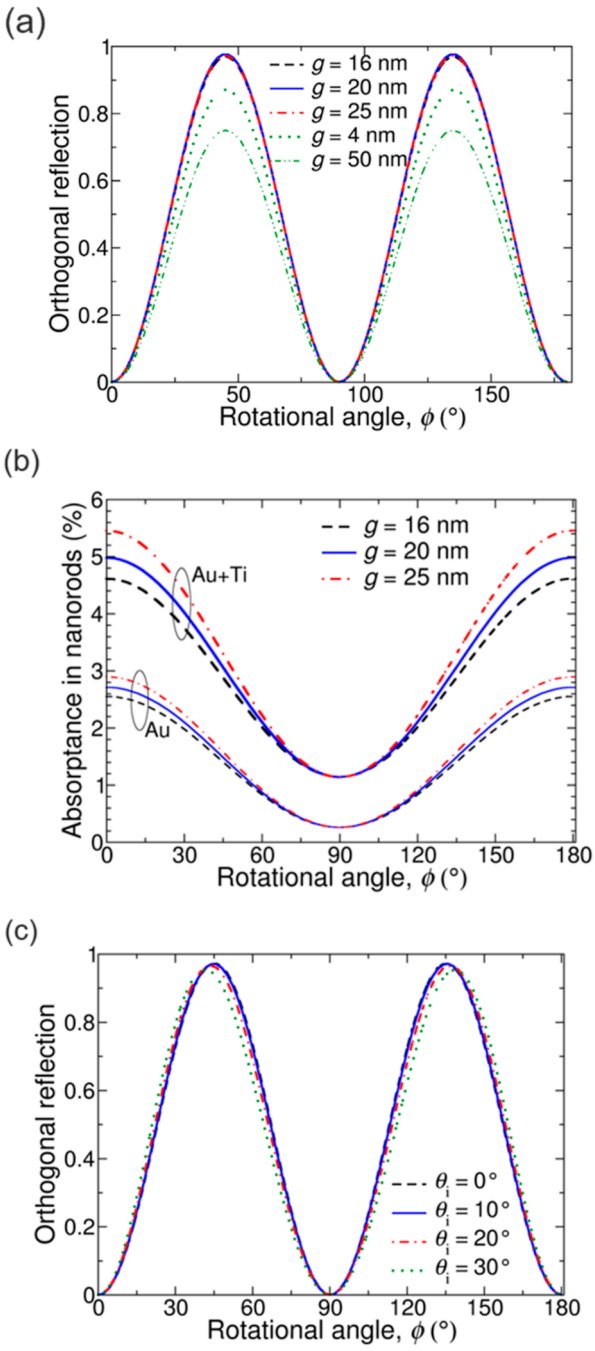

Figure 2. Full-wave 3D EM simulations at λ = 1550 nm for metasurface devices with a_x = 90 nm, a_y = 262 nm − g, a_z = 50 nm, p_x = 252 nm, and t_{SiO2} = 160 nm. (a) Simulated power relative to the incident power, reflected to the polarization orthogonal to that of the incident wave for g = 16, 20, 25, 4, and 50 nm with θ_i = 0, (b) absorption losses in the Au nanorods, including the Ti adhesion layer, and the losses in Au only for g = 16, 20, and 25, and (c) simulated power relative to the incident power, reflected to the polarization orthogonal to that of the incident wave for different θ_i with g = 20 nm. All of the curves are shown as a function of the rotational angle (ϕ) of the metasurface.

and ϕ = 135°, as can be seen in Figure 2b. It is notable that the contribution of the thin adhesion layer is relatively high, i.e., roughly half of the losses at the ϕ angles, where the maxima occur and even being the main contributor at ϕ = 90°. Variation of the interelement gap (g) has a very small effect on

https://doi.org/10.1021/acsomega.4c04158
ACS Omega 2024, 9, 33055−33063

the amount of polarization rotation and the insertion loss for g = 16−25 nm and for the θ_i angles of interest. This suggests that small deviations from the targeted values, which may occur in the fabrication, are well tolerated. However, larger deviations (g = 4 or 50 nm in Figure 2) can significantly affect the performance. The metasurface works efficiently for a broad range of angles of incidence, as shown for the simulated reflected power in Figure 2c.

To study the coupling losses of the on-chip PR of different thicknesses, two-dimensional (2D) simulations were performed for the system shown in Figure 3a. It represents the thick silicon waveguide terminated with URM and an isotropic material block representing a reflective waveplate that is placed on top of URM. Figure 3b,c shows the results of the 2D simulations for the system. The thick waveplate corresponds to a conventional waveplate, and the thin one imitates the case of the proposed metasurface. The electric field profile in a cross-sectional view is shown in Figure 3b. As there is no lateral guiding structure in the waveplate, the beam begins to diverge as it enters the plate. The amount of beam divergence and the corresponding coupling loss increase with the thickness of the waveplate. In Figure 3c, the power reflectance, or S_{11}, corresponding to the coupling efficiency, is shown as a function of the thickness of the waveplate. The coupling efficiency is less than −6 dB already at the thicknesses less than 15 μm, and preferably, the thickness should be well below 2 μm for relevant applications.

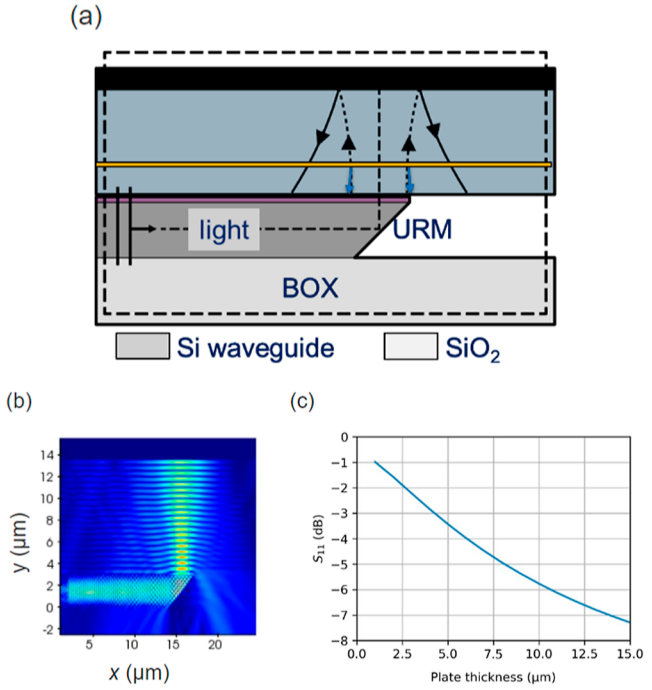

Figure 3. Coupling studies with 2D simulations. (a) Cross-sectional schematic image of the 45° URM in the Si waveguide showing the divergence of the reflected beam for a thick (black solid lines with arrows) and thin (blue solid lines with arrows) reflective waveplate. (b) Cross-sectional view of the simulated electric field profile for the system shown in (a). (c) Simulated reflectance, or S_{11}, corresponds to the coupling efficiency of the light from the reflective waveplate back to the waveguide via a URM, shown as a function of the thickness of the waveplate.

3.2. Free-Space Metasurface Devices without Silicon Waveguides. A metasurface waveplate device exhibiting PER more than 15 dB for a broad spectral range (120 nm) is shown in Figure 4a. Considering the 20 dB PER measured for a planar gold surface, it can be concluded that the metasurface imperfections contribute to about 2/3 of the total 3% of the input light coupled with the wrong polarization at the output. A strong polarization rotation with PCE between 91 and 98.5% is observed for all the studied devices. The PERs of the metasurfaces with different interelement gaps (g = 16−25 nm) are very similar, showing a conversion efficiency higher than 90% for a wavelength range larger than 100 nm. The measurements suggest that a small variation in the gaps between the nanorods does not have a significant influence on PER, which is in excellent agreement with the simulations (see Figure 2). Furthermore, to study the effect of the rotational angle of the metasurface with respect to the polarization of incident light, the input polarization maintaining fiber (PMF) is rotated with 5° steps, and the corresponding optical power is measured at the detector. The maximum optical power is

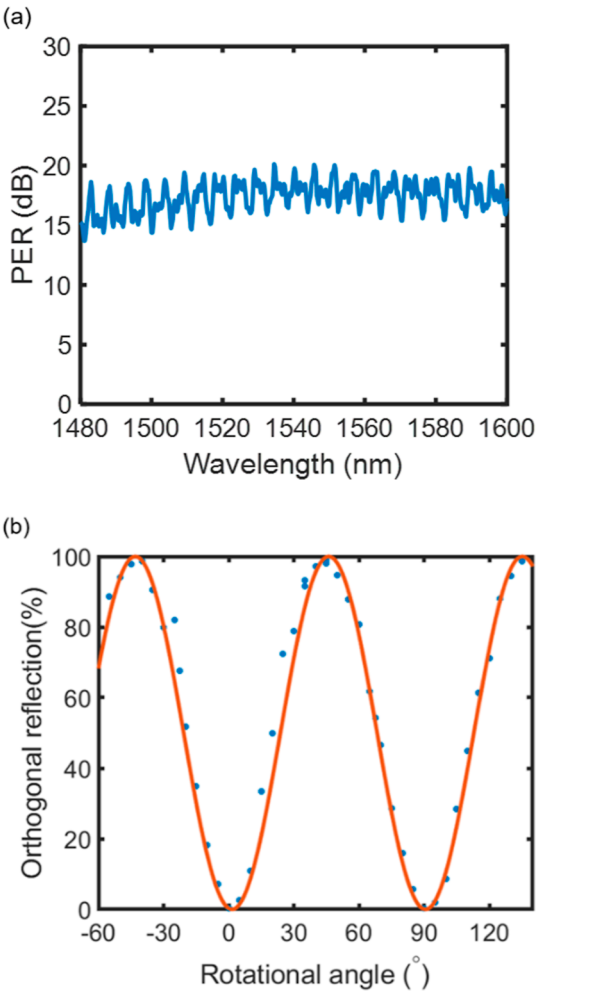

Figure 4. Free-space metasurface waveplate measurements. (a) Example of a PER measurement from a metasurface device after 90° rotation as a function of wavelength. (b) Measured reflected power (blue dots) for the polarization orthogonal to that of the incident wave as a function of the rotational angle, ϕ (changed by rotating the input PMF), and a sinusoidal fit to the results (orange solid line).

https://doi.org/10.1021/acsomega.4c04158
ACS Omega 2024, 9, 33055−33063

observed at $\phi = 45°$ or at its even multiples, as light undergoes the phase shift two times. Figure 4b shows the measured results and a sinusoidal fit of the data. The results are again in excellent agreement with the simulations.

3.3. Waveguide-integrated Metasurface-Based Polarization Rotator Measurements. Figure 5 shows the PER measured for a waveguide-integrated polarization rotator as a function of the wavelength. More than 10 dB PER was observed over the 120 nm bandwidth for the waveguide-integrated PR. Unwanted reflections from the input facet of the waveguide and the mirror surface reduce the achieved extinction ratio compared with that of the PER of the plain metasurface waveplate device shown in Figure 4a. This can be improved by further optimizing antireflection coatings for this application and using a tilted waveguide facet at the input. The single-layer antireflection coatings cannot suppress reflections over this broad wavelength range, which causes some of the light to experience two or more polarization rotations, especially at the left and right edges of the spectrum, as shown in Figure 5.

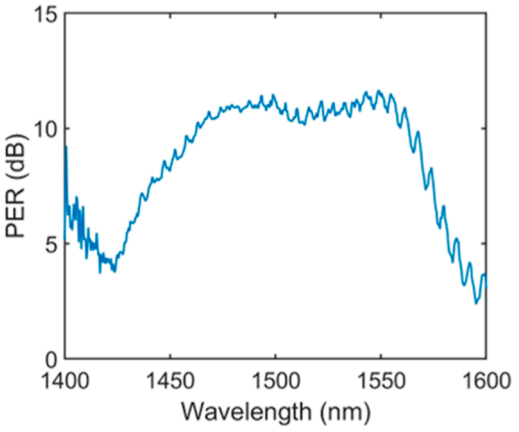

Figure 5. PER as a function of wavelength for a waveguide integrated polarization rotator showing more than 10 dB of PER for a bandwidth of 120 nm.

The waveguide-integrated PR device exhibits an overall loss of 8−10 dB, as illustrated in Figure 6a. This total loss encompasses various factors, including the coupling of the waveguide and URM, the intrinsic loss of the metasurface, coupling from URM to the metasurface and back, and scattering losses. The waveguide structure with a URM (without metasurface) has a coupling loss of 1.5−2.5 dB compared to the fiber-to-fiber case for the whole wavelength range (1400−1600 nm) as shown in Figure 6b for both polarizations. This loss only includes coupling from a waveguide to a fiber though an URM, i.e., no reflection back to the waveguide. Hence, the total loss for this structure, in our case, will be twice the value of 2.5 dB, accounting for the fact that light undergoes coupling to and from the URM. The standalone metasurface exhibits losses below 1.5 dB for both polarizations for the wavelength range of 1450−1630 nm compared to a planar gold surface (coupled with PMF), as shown in Figure 6c. The measured loss values are of the same order of magnitude but somewhat higher than the simulated values for the wavelength range close to 1550 nm. The simulated intrinsic loss of the nanorods is 3.5% at 1550 nm for $\phi = 45°$, which is in excellent agreement with the measured losses of 3.5% at 1563 nm for the TM polarization. The small differences can be explained by the irregularities and surface roughness occurring in the fabricated Au nanorod arrays compared with the simulated ideal geometries.

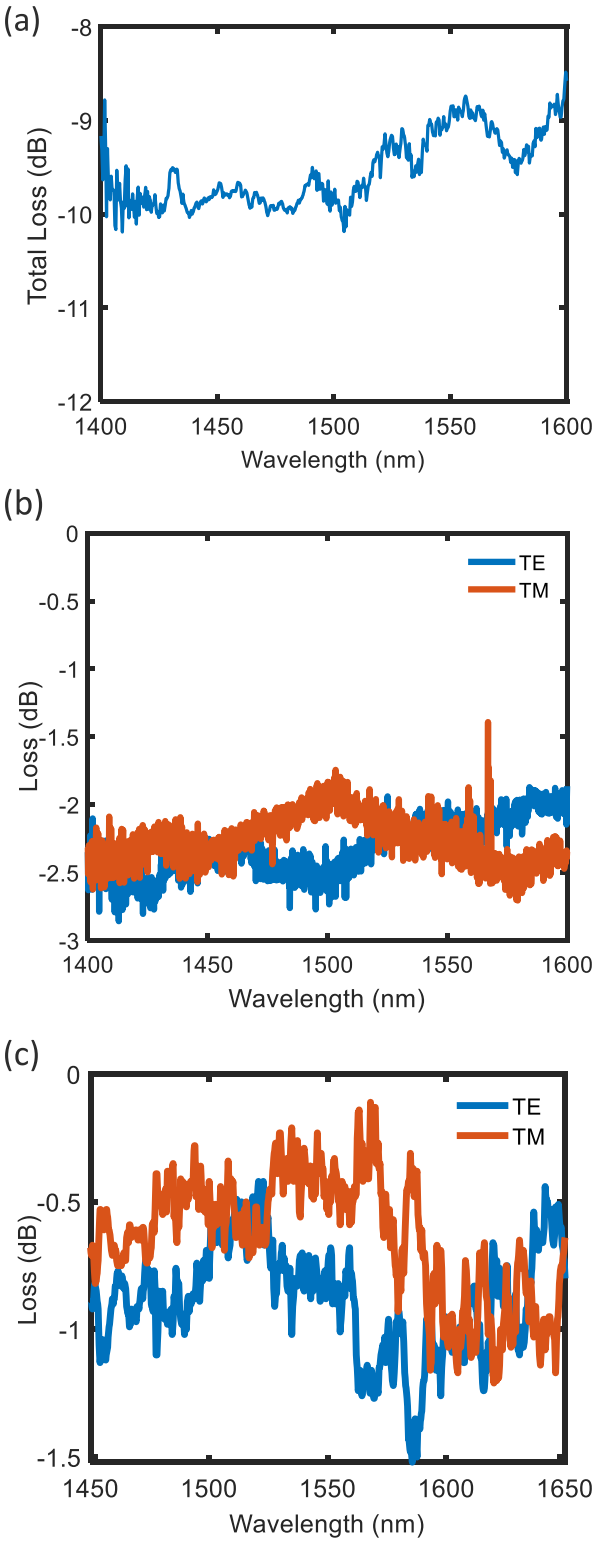

Figure 6. Loss analysis. (a) Total loss of a waveguide-integrated polarization rotator device. (b) Waveguide coupling losses without a metasurface on top of URM compared to the fiber-to-fiber case. (c) Losses of a standalone metasurface compared to a planar gold surface with TE referring to $\phi = 45°$ and TM referring to $\phi = -45°$.

https://doi.org/10.1021/acsomega.4c04158
ACS Omega 2024, 9, 33055−33063

Assuming waveguide losses of 4−5 dB, as mentioned earlier, and 4 dB coupling losses from the URM to the metasurface and back to the URM, including the intrinsic losses of the metasurface, the total loss would be 9 dB, which is in good agreement with the measured losses in Figure 6a. This explains the reduction in PER observed in the waveguide-integrated polarization rotator device compared to a standalone PR metasurface, as can be seen by comparing Figure 5 to Figure 4a. The total loss analysis suggests that approximately 7.2 dB, i.e., 80% of the total loss, is due to coupling and propagation to and from the metasurface and URM, while the remaining 1.8 dB loss, i.e., 20% of the total loss is attributed to the intrinsic loss of the nanorods and scattering.

The measured PER of the device is lower than the measured free-space metasurface PER due to waveguide losses and coupling loss between URM and the metasurface. The loss analysis of the metasurface losses agrees well with the simulated losses, reflecting the difference in the PER.

The oscillations observed in the measurements are due to the back reflections from the facets of the waveguide and fiber optic polarization splitter with a limited extinction ratio of 25 dB used in the measurement setup to ensure the injection of one of the orthogonal polarization states into the device.

4. CONCLUSIONS

We have demonstrated a gold-based metasurface waveplate device with high performance over a broad wavelength range (120 nm) with a PCE over 98.5%. We also proposed and demonstrated an approach that provides a gateway to miniaturized optical devices enabling compact and broadband PR on a thick-SOI platform. With the implemented metasurfaces, we have successfully demonstrated a compact on-chip polarization rotator using nanorods on top of an up-reflecting mirror on a thick-SOI waveguide platform. To the best of our knowledge, this is the first demonstration of the successful integration of a functional metasurface on a PIC for on-chip polarization management.

The demonstrated proof-of-concept devices still have certain challenges, such as the alignment of the metasurface chip on top of a silicon waveguide chip. A practical solution for a compact device is to use flip-chip bonding and transfer printing techniques,[38] or as the most compact solution, to fabricate the reflective metasurface directly on the horizontal surface of the URM. Further, to implement a device that is more useful from the application point of view, such as PR serving as a Pauli-Z gate for quantum computing,[39] more advanced designs are needed in which different waveguides are used as input and output, e.g., a Michelson interferometer based on a 50:50 splitter.

In this paper, we focused on plasmonic metal surfaces to achieve polarization rotation. Even though these metasurfaces are compact and have high optical confinement, they still somewhat suffer from intrinsic optical losses (~3.5%), which may limit the efficiency of high-performance optical devices. This could be improved by resorting to all-dielectric metasurfaces, for example, a metasurface made of amorphous silicon, a material readily available in the thick-SOI platform.[40] The losses of the waveguides can be mitigated by using hydrogen annealed waveguides for reducing the surface wall roughness of the waveguides.[41] Further, the coupling efficiency between the metasurface and waveguide may be improved by leveraging the resonant modes of a metasurface by matching the resonant modes of the metasurface to the guided modes of the waveguide.[42,43]

5. METHODS

5.1. Numerical Simulations. Three-dimensional (3D) full-wave electromagnetic (EM) simulations of the geometry in Figure 1 were carried out to optimize the plasmonic metasurface design for the targeted wavelength (λ) range

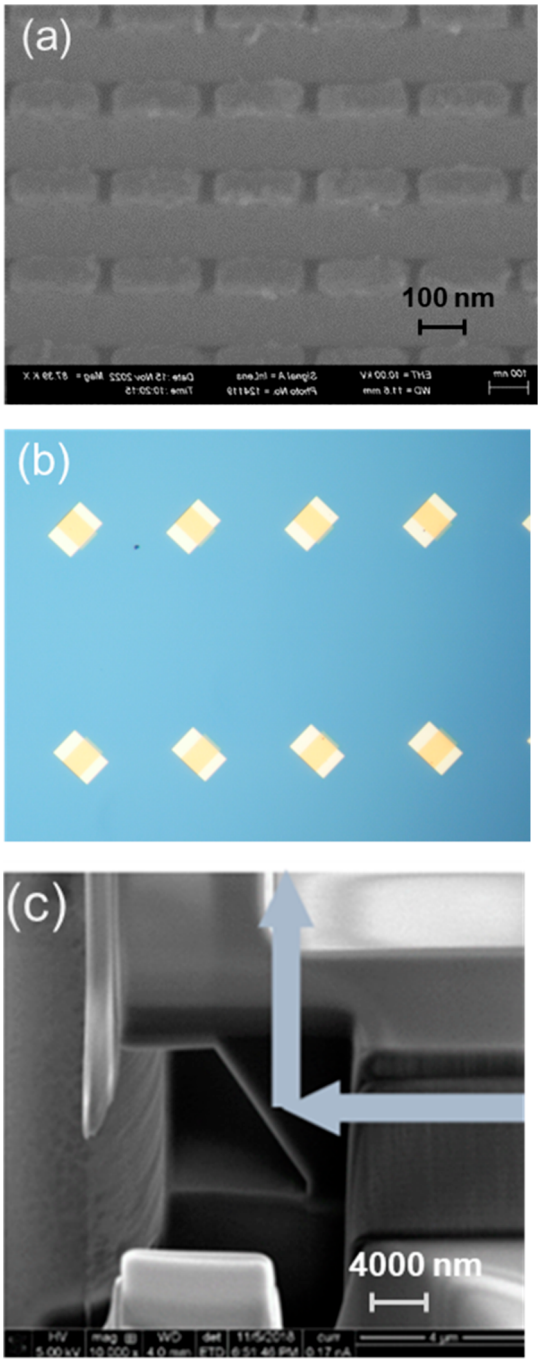

Figure 7. Microscope and SEM images of the plasmonic metasurfaces and URMs. (a) SEM image of 242 × 90 nm rectangular-shaped plasmonic nanorods. (b) Microscope image of a chip with plasmonic metasurface devices (eight devices visible on top of the 20 × 30 μm gold mirrors). (c) A SEM image of an URM.

https://doi.org/10.1021/acsomega.4c04158
ACS Omega 2024, 9, 33055−33063

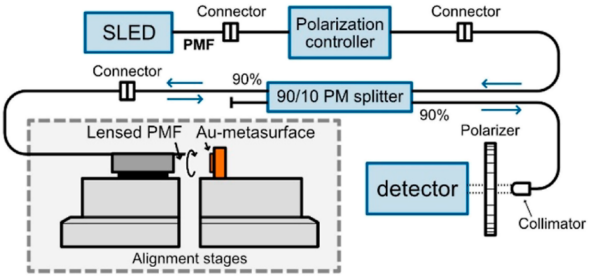

Figure 8. Measurement setup to measure the standalone metasurface device in reflection mode without the silicon photonics waveguide. The multiaxis stages are used for the alignment, and the lensed PMF fiber is rotated during the measurements.

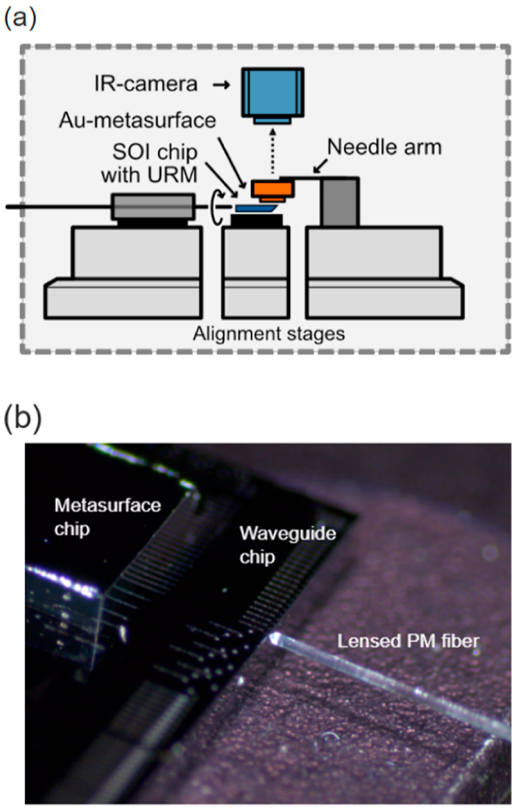

Figure 9. (a) Measurement setup to measure the metasurface-based PR integrated with silicon photonics waveguides. The multiaxis stages are used for the alignment, and the lensed PMF fiber is rotated during the measurements. The rest of the setup (outside the dashed box) is equivalent to the one in Figure 8. (b) Microscope image of a PMF coupled with a silicon waveguide and a metasurface chip on top of the silicon photonics waveguide.

near 1550 nm with the Wave Optics module of COMSOL Multiphysics.[44]

Periodic boundary conditions were used for the sides of the simulation region to imitate an infinite lattice of gold rods in the arrangement of the metasurface. It should be mentioned that the assumption of an infinite lattice is not justified for the waveguide-integrated case, considering the mode-field diameter of the beam (2.5 μm), its divergence angle, and the period of the metasurface (524 nm). However, the mode can be considered as an expansion of infinite plane waves incident at different θ_i angles at the metasurface, the acceptance angle of which is larger than the largest θ_i of the mode (15 ± 1°). By adjustment of the size of the gold rod and the x and y dimensions of the simulation region, different metasurface designs with different periods and distances between the rods could be tested in addition to the varied thicknesses of the SiO_2 and Au layers. A linearly polarized plane wave was used as the EM wave incident on the Au-rods from a port in the air, and the polarization state and the power of the reflected wave were monitored at the same port position.

In addition to the 3D simulations, two-dimensional (2D) EM simulations were carried out to compare the coupling losses of the proposed metasurface structure to those of a conventional reflective waveplate on top of the URM. The simulations were performed using a 2D FDTD solver in Ansys Lumerical[45] for the structure shown in Figure 3a. The back surface of the waveplate is metallized, which reflects the light back to the waveguide via the same URM. The URM has an antireflection coating of 195 nm of Si_3N_4 with a refractive index of 2.0, and there is a fixed 100 nm air gap between the URM and the waveplate. The refractive index of the waveplate is isotropic and has a value of 1.5. Light is launched into the fundamental mode of the Si waveguide, and the device loss is determined by calculating the amount of power coupled back to the fundamental mode.

5.2. Fabrication Process. A 150 mm p-type silicon wafer is used as a substrate for the fabrication of the metasurface-based polarization rotator waveplates. The design layout produces 100 chips 2.0 × 2.5 mm in size. Each chip consists of 16 metasurface devices arranged in two rows. The chip with the polarization rotator devices is designed to match the layout of silicon photonic chips having waveguides with URMs.

As the first step, 1.5 μm deep alignment marks are fabricated into the silicon substrate by electron beam lithography (EBL) and dry etching. Then, EBL and lift-off processes are used to define 20 × 30 μm mirrors onto the substrate. For this, a gold layer of a thickness of 100 nm is deposited with a 2 nm titanium (Ti) adhesion layer on top of the patterned resist by evaporation followed by a lift-off in acetone with the assistance of ultrasonic agitation, leaving the 20 by 30 μm gold mirrors on the surface. The mirror layer is then covered by a 160 nm thick layer of silicon oxide (t_{SiO2}) using Oxford Plasmalab Plasma-enhanced chemical vapor deposition (PECVD) equipment.

The metasurface consisting of submicrometer scale rectangles (nanorods) in arrays is finally defined on top of the dielectric by EBL and lift-off process. A 50 nm-thick layer of Au with a Ti adhesion layer is evaporated on a patterned EBL resist prior to an acetone bath with ultrasonic agitation. The metasurface dimensions of the fabricated devices are as follows: a_x = 90 nm, $a_y = p_y - g$, and a_z = 50 nm with g = 16–25 nm, while the period in x direction p_x = 252 nm and in y direction p_y = 262 nm. As the final step, lanes are formed into oxide by EBL and dry etching to prevent oxide chipping or peeling during dicing. A SEM image of a fabricated metasurface and a microscopic image of the metasurfaces arranged on a chip are presented in Figure 7a,b, respectively.

The 3 μm SOI waveguides and URMs were fabricated on separate wafers with a combination of dry and wet etching. A SEM image of a 45° mirror is shown in Figure 7c.

5.3. Optical Measurements. *5.3.1. Characterization of Standalone-Metasurfaces.* To measure the PER of the metasurface waveplate devices, we used the optical fiber-based setup presented in Figure 8. A superluminescent diode (SLED) at λ = 1550 nm is used as a light source in the PER measurements, whereas rotation angle-dependent measure-

https://doi.org/10.1021/acsomega.4c04158
ACS Omega 2024, 9, 33055−33063

ments are carried out using an erbium-doped fiber amplifier as a spontaneous emission source. The light is polarized and directed toward the metasurface via a polarization maintaining (PM) 10/90 coupler using a lensed PMF. The coupler is used to separate a part of the reflected light for the measurements. The coupler has low polarization dependence as compared to a circulator and works regardless of which polarization axis of the fiber (slow or fast) the light is connected to. The alignment stages shown in Figure 8 are used to align the PMF and the metasurface waveplate.

The capability of the setup to measure the maximum PER was first checked with reference measurements on a planar gold surface. The reference measurements produced a PER of more than 20 dB for the whole wavelength range studied (1480−1650 nm) without any polarization rotation. The maximum PER is limited to 20−25 dB by the finite PER of the PMF and the PM splitter in the setup. After optimizing the power and angle, the power of the two orthogonal polarizations ($P_{\phi 1}$ and $P_{\phi 2}$) reflected from the Au metasurface devices were measured and the PER was calculated using eq 1.

$$\mathrm{PER} = 10 \log_{10} \frac{P_{\phi_2}}{P_{\phi_1}} (\mathrm{dB}) \tag{1}$$

where $P_{\phi 1}$ and $P_{\phi 2}$ describe the power of the reflected wave polarized along $\phi_1 = 45°$ and $\phi_2 = -45°$, respectively, when the incident wave is polarized along $\phi_1 = 45°$. The PER measurements were carried out on multiple samples. The maximum reflected power for the orthogonal polarizations is observed at $\phi = \pm 45°$. Thus, the total rotational angle between the input and output polarizations is 90°.

5.3.2. Characterization of Waveguide-integrated Polarization Rotator. For the measurements of the waveguide integrated polarization rotator, a gold metasurface chip is placed on top of the URM of a silicon waveguide. The metasurface chip is glued to a needle and then aligned with the waveguide chip. The measurement setup is shown in Figure 9a. The active alignment is done with the help of an infrared (IR) camera. Figure 9b shows a microscopic image of a PMF coupled with a silicon waveguide and a metasurface chip on top of the silicon photonic waveguide chip. The light is injected by using the PMF to match the optical axis of the waveguide.

AUTHOR INFORMATION

Corresponding Authors

Dura Shahwar − *VTT Technical Research Centre of Finland Ltd, 02150 Espoo, Finland; QTF Centre of Excellence, Department of Electronics and Nanoengineering, Aalto University, 02150 Espoo, Finland;* orcid.org/0000-0002-3187-3619; Email: dura.shahwar@vtt.fi

Kirsi Tappura − *VTT Technical Research Centre of Finland Ltd, 02150 Espoo, Finland; QTF Centre of Excellence, VTT Technical Research Centre of Finland Ltd, FI-02044 VTT Espoo, Finland;* orcid.org/0000-0002-8032-9652; Email: kirsi.tappura@vtt.fi

Authors

Markku Kapulainen − *VTT Technical Research Centre of Finland Ltd, 02150 Espoo, Finland*

Tomi Haatainen − *VTT Technical Research Centre of Finland Ltd, 02150 Espoo, Finland*

Mikko Harjanne − *VTT Technical Research Centre of Finland Ltd, 02150 Espoo, Finland*

Matteo Cherchi − *VTT Technical Research Centre of Finland Ltd, 02150 Espoo, Finland;* Present Address: Xanadu, Canada

Zhipei Sun − *QTF Centre of Excellence, Department of Electronics and Nanoengineering, Aalto University, 02150 Espoo, Finland;* orcid.org/0000-0002-9771-5293

Timo Aalto − *VTT Technical Research Centre of Finland Ltd, 02150 Espoo, Finland*

Complete contact information is available at: https://pubs.acs.org/10.1021/acsomega.4c04158

Author Contributions

D.S. and K.T. conceived and designed the project inspired by discussions with M.C. D.S. and M.K. performed the experimental characterization and analyzed the measurement results. K.T. carried out numerical simulations for the metasurfaces. M.H. performed the numerical simulations for conventional waveplates. T.H. fabricated the metasurfaces. T.A. and M.C. supported the interpretation of the results. All the authors contributed to the manuscript which was originally written by D.S. and K.T with the help of T.H., M.K., and M.H. Z.S., T.A., M.C., and K.T. reviewed and edited the manuscript. All the authors discussed the results and commented on the manuscript. All the work was carried out under the supervision of K.T.

Funding

Academy of Finland Project Novel optical isolators to continue Moore's law in photonics integration (NOIMO) (Decision number 333980) and the Academy of Finland Flagship Programme, Photonics Research, and Innovation (PREIN) (Decision number 346545).

Notes

The authors declare no competing financial interest.

ACKNOWLEDGMENTS

Authors would like to thank fabrication experts at VTT Technical Research Centre of Finland.

REFERENCES

(1) Huang, L.; Chen, X.; Mühlenbernd, H.; Li, G.; Bai, B.; Tan, Q.; Jin, G.; Zentgraf, T.; Zhang, S. Dispersionless Phase Discontinuities for Controlling Light Propagation. *Nano Lett.* **2012**, *12* (11), 5750−5755.

(2) yu, N.; Genevet, P.; Kats, M.; Aieta, F.; Tetienne, J.-P.; Capasso, F.; Gaburro, Z. Light Propagation with Phase Discontinuities: Generalized Laws of Reflection and Refraction. *Science* **2011**, *334*, 333−337.

(3) Hu, Y.; Wang, X.; Luo, X.; Ou, X.; Li, L.; Chen, Y.; Ping, Y.; Wang, S.; Wang, S.; Duan, H. All-Dielectric Metasurfaces for Polarization Manipulation: Principles and Emerging Applications. *Nanophotonics* **2020**, *9* (12), 3755−3780.

(4) Chen, H.-T.; Taylor, A.; yu, N. A Review of Metasurfaces: Physics and Applications. *Rep. Prog. Phys.* **2016**, *79*, 076401.

(5) Khorasaninejad, M.; Capasso, F. Metalenses: Versatile Multifunctional Photonic Components. *Science* **2017**, *358*, No. eaam8100.

(6) Zhao, Z.; Pu, M.; Gao, H.; Jin, J.; Li, X.; Ma, X.; Wang, Y.; Gao, P.; Luo, X. Multispectral Optical Metasurfaces Enabled by Achromatic Phase Transition. *Sci. Rep.* **2015**, *5* (1), 15781.

(7) Zheng, G.; Mühlenbernd, H.; Kenney, M.; Li, G.; Zentgraf, T.; Zhang, S. Metasurface Holograms Reaching 80% Efficiency. *Nat. Nanotechnol.* **2015**, *10* (4), 308−312.

(8) Chu, H.; Li, Q.; Liu, B.; Luo, J.; Sun, S.; Hang, Z. H.; Zhou, L.; Lai, Y. A Hybrid Invisibility Cloak Based on Integration of Transparent Metasurfaces and Zero-Index Materials. *Light Sci. Appl.* **2018**, *7* (1), 50.
(9) Kim, M.; Lee, D.; Yang, Y.; Kim, Y.; Rho, J. Reaching the Highest Efficiency of Spin Hall Effect of Light in the Near-Infrared Using All-Dielectric Metasurfaces. *Nat. Commun.* **2022**, *13* (1), 2036.
(10) Karamirad, M.; Ghobadi, C.; Nourinia, J. Metasurfaces for Wideband and Efficient Polarization Rotation. *IEEE Trans. Antennas Propag.* **2021**, *69* (3), 1799−1804.
(11) Pouyanfar, N.; Nourinia, J.; Ghobadi, C. Multiband and Multifunctional Polarization Converter Using an Asymmetric Metasurface. *Sci. Rep.* **2021**, *11* (1), 9306.
(12) Kurosawa, H.; Choi, B.; Sugimoto, Y.; Iwanaga, M. High-Performance Metasurface Polarizers with Extinction Ratios Exceeding 12000. *Opt. Express* **2017**, *25* (4), 4446−4455.
(13) Jiang, Z. H.; Lin, L.; Ma, D.; Yun, S.; Werner, D. H.; Liu, Z.; Mayer, T. S. Broadband and Wide Field-of-View Plasmonic Metasurface-Enabled Waveplates. *Sci. Rep.* **2014**, *4* (1), 7511.
(14) Abouelatta, M.; Obayya, S.; Hameed, M. F. O. Highly Efficient Transmissive Metasurface for Polarization Control. *Opt. Quantum Electron.* **2021**, *53*, 87.
(15) Wu, Z.; Ra'di, Y.; Grbic, A. Tunable Metasurfaces: A Polarization Rotator Design. *Phys. Rev. X* **2019**, *9* (1), 011036.
(16) Zhao, Y.; Xiang, J.; He, A.; He, Y.; Guo, X.; Su, Y. Metamaterial-Enabled Fully On-Chip Polarization-Handling Devices. *Laser Photonics Rev.* **2023**, *17* (11), 2300320.
(17) Dai, D.; Liu, L.; Gao, S.; Xu, D.-X.; He, S. Polarization Management for Silicon Photonic Integrated Circuits. *Laser Photonics Rev.* **2013**, *7* (3), 303−328.
(18) Rahim, A.; Ryckeboer, E.; Subramanian, A. Z.; Clemmen, S.; Kuyken, B.; Dhakal, A.; Raza, A.; Hermans, A.; Muneeb, M.; Dhoore, S.; Li, Y.; Dave, U.; Bienstman, P.; Le Thomas, N.; Roelkens, G.; Van Thourhout, D.; Helin, P.; Severi, S.; Rottenberg, X.; Baets, R. Expanding the Silicon Photonics Portfolio With Silicon Nitride Photonic Integrated Circuits. *J. Light. Technol.* **2017**, *35* (4), 639−649.
(19) Cherchi, M.; Bera, A.; Kemppinen, A.; Nissilä, J.; Tappura, K.; Caputo, M.; Lehtimäki, L.; Lehtinen, J.; Govenius, J.; Aalto, T. Supporting Quantum Technologies with a Micron-Scale Silicon Photonics Platform. In *Proceedings Volume 12004, Integrated Optics: Devices, Materials, and Technologies XXVI*; SPIE OPTO, 2022.
(20) Liu, B.; Shum, P.; Zhang, J.; Lo, G.-Q.. Fabrication Tolerance Study on Mode-Coupling-Based Polarization Rotators. In *2010 IEEE International Conference on Communication Systems*; IEEE, 2010; pp 681−684. .
(21) Xie, A.; Zhou, L.; Chen, J.; Li, X. Efficient Silicon Polarization Rotator Based on Mode-Hybridization in a Double-Stair Waveguide. *Opt. Express* **2015**, *23* (4), 3960−3970.
(22) Watts, M. R.; Haus, H. A. Integrated Mode-Evolution-Based Polarization Rotators. *Opt. Lett.* **2005**, *30* (2), 138−140.
(23) Wang, S.; Li, P.; Yan, J. Monolithically Integrated Polarization Rotator and Splitter with Designed Power Ratio. *Opt. Express* **2023**, *31* (9), 14128−14139.
(24) Ito, M.; Fukui, T.; Tanemura, T.; Nakano, Y. Compact Symmetric Polarization Rotator-Splitter on InP. *Opt. Express* **2022**, *30* (3), 4179−4188.
(25) Shahwar, D.; Cherchi, M.; Harjanne, M.; Kapulainen, M.; Aalto, T. Polarization Splitters for Micron-Scale Silicon Photonics. In *International Society for Optics and Photonics*; SPIE; 2021; Vol. *11691*, p 1169104. .
(26) Suzuki, Y.; Elfiqi, A. E.; Fukui, T.; Ito, M.; Tanemura, T.; Nakano, Y.. V-Groove-Assisted Polarization Splitter-Rotator on Multi-Micron Silicon Photonics. In *2022 27th OptoElectronics and Communications Conference (OECC) and 2022 International Conference on Photonics in Switching and Computing (PSC)*; IEEE, 2022; pp 1−3. .
(27) Liu, L.-Y.; Huang, H.-C.; Chen, C.-W.; Hsiao, F.-L.; Cheng, Y.-C.; Chen, C.-C. Design of Reflective Polarization Rotator in Silicon Waveguide. *Nanomaterials* **2022**, *12* (20), 3694.
(28) Gao, L.; Huo, Y.; Zang, K.; Paik, S.; Chen, Y.; Harris, J. S.; Zhou, Z. On-Chip Plasmonic Waveguide Optical Waveplate. *Sci. Rep.* **2015**, *5* (1), 15794.
(29) Hou, Z.-S.; Xiong, X.; Jia-Ji, C.; Chen, Q.-D.; Tian, Z.-N.; Ren, X.-F.; Sun, H.-B. On-Chip Polarization Rotators. *Adv. Opt. Mater.* **2019**, *7*, 1900129.
(30) Xu, H.; Dai, D.; Shi, Y. Anisotropic Metamaterial-Assisted All-Silicon Polarizer with 415-Nm Bandwidth. *Photonics Res.* **2019**, *7* (12), 1432−1439.
(31) Meng, Y.; Chen, Y.; Lu, L.; Ding, Y.; Cusano, A.; Fan, J. A.; Hu, Q.; Wang, K.; Xie, Z.; Liu, Z.; Yang, Y.; Liu, Q.; Gong, M.; Xiao, Q.; Sun, S.; Zhang, M.; Yuan, X.; Ni, X. Optical Meta-Waveguides for Integrated Photonics and Beyond. *Light Sci. Appl.* **2021**, *10* (1), 235.
(32) Guo, X.; Ding, Y.; Chen, X.; Duan, Y.; Ni, X. Molding Free-Space Light with Guided Wave-Driven Metasurfaces. *Sci. Adv.* **2020**, *6*, No. Eabb4142.
(33) Zhong, H.; Zheng, Y.; Sun, J.; Wang, Z.; Zhang, L.; Liang, Y.; Hua, Q.; Ning, M.; Ji, J.; Fang, B. Gigahertz-Rate-Switchable Wavefront Shaping through Integration of Metasurfaces with Photonic Integrated Circuit. **2023**, arXiv:231108867. arXiv Preprint.
(34) Hsieh, P.-Y.; Fang, S.-L.; Lin, Y.-S.; Huang, W.-H.; Shieh, J.-M.; Yu, P.; Chang, Y.-C. Metasurfaces on Silicon Photonic Waveguides for Simultaneous Emission Phase and Amplitude Control. *Opt. Express* **2023**, *31* (8), 12487−12496.
(35) Kamali, S. M.; Arbabi, E.; Arbabi, A.; Faraon, A. A Review of Dielectric Optical Metasurfaces for Wavefront Control. *Nanophotonics* **2018**, *7* (6), 1041−1068.
(36) Li, Z.; Kim, M.-H.; Wang, C.; Han, Z.; Shrestha, S.; Overvig, A. C.; Lu, M.; Stein, A.; Agarwal, A. M.; Lončar, M.; et al. Controlling Propagation and Coupling of Waveguide Modes Using Phase-Gradient Metasurfaces. *Nat. Nanotechnol.* **2017**, *12* (7), 675−683.
(37) Aalto, T.; Cherchi, M.; Harjanne, M.; Bhat, S.; Heimala, P.; Sun, F.; Kapulainen, M.; Hassinen, T.; Vehmas, T. Open-Access 3-Mm SOI Waveguide Platform for Dense Photonic Integrated Circuits. *IEEE J. Sel. Top. Quantum Electron.* **2019**, *25* (5), 1−9.
(38) Shi, W.; Zou, C.; Cao, Y.; Liu, J. The Progress and Trend of Heterogeneous Integration Silicon/III-V Semiconductor Optical Amplifiers. *Photonics* **2023**, *10* (2), 161.
(39) Heilmann, R.; Gräfe, M.; Nolte, S.; Szameit, A. Arbitrary Photonic Wave Plate Operations on Chip: Realizing Hadamard, Pauli-X and Rotation Gates for Polarisation Qubits. *Sci. Rep.* **2014**, *4* (1), 4118.
(40) Khorasaninejad, M.; Crozier, K. B. Polarization Splitting at Infrared Wavelengths Using Silicon Nanoridges. *In 2014 Conference on Lasers and Electro-Optics (CLEO) - Laser Science to Photonic Applications*; Optica Publishing Group: San Jose, CA, 2014; p SF1O.1..*CLEO: 2014; OSA Technical Digest (online)*
(41) Marin, Y. E.; Bera, A.; Cherchi, M.; Aalto, T. Ultra-High-Q Racetrack Resonators on Thick SOI Platform Through Hydrogen Annealing Smoothing. *J. Light. Technol.* **2023**, *41* (11), 3642−3648.
(42) Huang, L.; Jin, R.; Zhou, C.; Li, G.; Xu, L.; Overvig, A.; Deng, F.; Chen, X.; Lu, W.; Alù, A.; et al. Ultrahigh-Q Guided Mode Resonances in an All-Dielectric Metasurface. *Nat. Commun.* **2023**, *14* (1), 3433.
(43) Yang, Z.; Jin, D. Polarized Upconversion Emission at Metasurface. *Light Sci. Appl.* **2023**, *12* (1), 263.
(44) *COMSOL Multiphysis®*, version 6.0, Www.Comsol.Com.
(45) Lumerical Solution Inc.. Available: http://www.lumerical.com.

https://doi.org/10.1021/acsomega.4c04158
ACS Omega 2024, 9, 33055−33063